Journal of Electronic Materials (2024) 53:5130–5141
https://doi.org/10.1007/s11664-024-11176-9

28TH INTERNATIONAL CONFERENCE ON NUCLEAR TRACKS AND RADIATION MEASUREMENTS

Synthesis, Characterization, and Enhanced Photocatalytic Degradation of Rose Bengal (RB) Dye Using an α-Fe_2O_3/MgO Nanocomposite

Sonia[1] · Manoj Kumar Srivastava[2] · V. Agarwal[3] · Harita Kumari[4] · Sourabh Sharma[5] · Monica[1] · Rakesh Kumar[6] · Surjeet Chahal[7]

Received: 16 March 2024 / Accepted: 9 May 2024 / Published online: 5 June 2024

Abstract

The current investigation delves into the structural, morphological, optical, and magnetic properties of α-Fe_2O_3, MgO, and an α-Fe_2O_3/MgO nanocomposite, synthesized via an innovative hydrothermal methodology, offering novel insights into their potential application in the purification of dye-contaminated water. Through meticulous analysis, x-ray diffraction (XRD) patterns authenticate the successful formation of the nanocomposite, while high-resolution transmission electron microscopy (HRTEM) reveals nanocrystalline particles with dimensions ranging from 19 nm to 30 nm. A noteworthy observation is the demonstration of a tunable optical bandgap, spanning from 2.20 eV to 3.08 eV, via UV–visible (UV–Vis) spectroscopy, indicative of the integration of wide-bandgap semiconductors, a key feature essential for efficient photocatalytic activity. Evaluation of the magnetic properties using vibrating sample magnetometry (VSM) shows a discernible reduction in magnetization in the nanocomposite, attributed to the incorporation of nonmagnetic MgO into the magnetic α-Fe_2O_3 matrix, thereby revealing unprecedented magnetic modulation. Particularly striking is the exceptional photocatalytic performance of the α-Fe_2O_3/MgO nanocomposite, achieving 84% degradation of rose Bengal (RB) dye under UV light exposure within a remarkably brief 75-min period. This pronounced enhancement in photocatalytic activity is ascribed to the reduced recombination probability of photo-induced carriers, suggesting effective charge transfer within the nanocomposite, thus elucidating its suitability for efficient wastewater treatment, particularly in the domain of dye removal.

Keywords Nanocomposite · rose Bengal · degradation · hydrothermal · photocatalysis · wastewater

Introduction

Water pollution poses a significant threat to the ecological community, fueled primarily by industrialization leading to the contamination of water resources with harmful pollutants. The prolonged scarcity of water intensifies this concern.[1,2] Notably, a variety of organic and inorganic dyes, utilized in industries such as textiles, pharmaceuticals, food, plastics, and paper, contribute as significant contaminants in water sources.[3] Among the array of dyes used in industries, rose Bengal (RB) dye poses a difficult challenge for elimination from waste water due to its widespread use and persistence. RB, belonging to the carcinogenic xanthene group, is a highly toxic dye.[4] The harmful impact of RB includes severe effects on the corneal epithelium, leading to various health issues such as itchiness, irritation, and blistering of eyes upon skin contact.[5]

✉ Surjeet Chahal
chahalsurjeet42@gmail.com

1 Department of Physics, Deenbandhu Chhotu Ram University of Science and Technology, Murthal, Haryana 131039, India

2 Department of Physics, D.A.V. P.G. College, D.D.U. Gorakhpur University, Gorakhpur, UP 273001, India

3 Department of Physics, Maitreyi College, University of Delhi, Chanakyapuri, Delhi 110021, India

4 Department of Physics, Maharshi Dayanand University, Rohtak, Haryana 124001, India

5 Department of Physics, Netaji Subhas University of Technology, Dwarka, Sec. 3, New Delhi 110078, India

6 Department of Physics, Kurukshetra University, Kurukshetra, Haryana 136119, India

7 Department of Physics, University Centre for Research and Development, Chandigarh University, Gharuan, Mohali 140413, India

Various techniques are used for the removal of dyes from wastewater such as adsorption, advanced oxidation, and ozonation. However, the complete removal of synthetic dyes, especially RB dye, from water remains a significant challenge.[6] According to several reports, inadequately managed wastewater can lead to significant repercussions for the ecosystem, posing a significant threat to the survival of numerous aquatic species and to human health.[7] Eliminating these contaminants from wastewater is the top priority for the scientific community.

The indiscriminate discharge of synthetic dyes into aquatic ecosystems poses a significant threat to environmental and human health. RB dye, a commonly used textile dye, is notorious for its persistence and adverse effects on aquatic organisms. Traditional treatment methods such as adsorption and biological degradation exhibit limited efficacy and often entail high operational costs. Thus, there is a pressing need for advanced and cost-effective approaches to mitigate dye pollution.

In the realm of water treatment technologies, there exists a discernible market gap characterized by the lack of economically viable and environmentally sustainable solutions for dye removal. Conventional methods suffer from drawbacks such as low efficiency, generation of toxic byproducts, and high energy consumption. Consequently, industries are in search of innovative alternatives capable of achieving rapid and complete degradation of dyes while minimizing resource utilization and environmental footprints.[8] The utilization of α-Fe_2O_3/MgO nanocomposites represents a promising avenue to address this market gap by offering a cost-effective and efficient solution for dye remediation.

Despite the considerable progress in photocatalytic materials for water treatment, several research gaps persist, hindering the widespread adoption of photocatalysis as a viable technology. One such gap lies in the development of photocatalysts with enhanced stability and recyclability, crucial factors for practical application. Furthermore, there is a need for comprehensive studies elucidating the underlying mechanisms governing the photocatalytic degradation process, including the role of nanocomposite morphology, surface properties, and reaction kinetics. By addressing these research gaps, α-Fe_2O_3/MgO nanocomposites hold the potential to revolutionize the field of photocatalysis and pave the way for sustainable water treatment solutions.

The α-Fe_2O_3/MgO nanocomposite, synthesized via hydrothermal method, exhibits exceptional photocatalytic activity towards the degradation of RB dye. The synergistic effect between α-Fe_2O_3 and MgO components enhances light absorption and promotes charge separation, leading to efficient generation of reactive oxygen species (ROS) responsible for dye degradation. Moreover, the nanocomposite's high surface area and tailored surface chemistry facilitate adsorption of RB molecules, thereby accelerating the photocatalytic process.[9]

Among the available techniques, photocatalysis stands out as particularly advantageous compared to other methods due to cost-effectiveness and low energy consumption. Photocatalysis is described as a mechanism that accelerates the transition of charged particles from the valence band to the conduction band in the presence a catalyst exposed to light.[10] This innovative green technology is based on advanced oxidation processes (AOP) and generates reactive species, playing an important role in the degradation of organic waste.[11,12] In this study, we employed a photocatalytic method to degrade dye molecules in wastewater. In recent years, the utilization of nanoparticles for dye removal from wastewater has gained prominence due to their large surface area, high adsorption properties, and faster equilibrium rates.

Numerous metal oxide semiconductors have been identified for the photocatalytic degradation of pollutants. These include various metal oxides such as ZnO, MgO, TiO_2, SnO_2, CeO_2, and ZrO_2 due to their unique electronic properties with adequate charge transfer capabilities that can initiate the degradation of pollutants in various environmental remediation processes.[13,14] α-Fe_2O_3 is a narrow-bandgap semiconductor with a range of 1.9–2.2 eV, serving as a donor. This is attributed to its tendency to transfer electrons to wide-bandgap semiconductors and excellent chemical stability, making it a promising option for water treatment. However, its limited application in photocatalysis is hindered by the relatively small bandgap, which results in the rapid recombination of electron–hole pairs.

To enhance its performance, combining α-Fe_2O_3 with a wide-bandgap semiconductor like MgO offers significant advantages.[15] Firstly, the potential for recombination of photo-excited electron–hole pairs is reduced. Secondly, the introduction of a wide-bandgap semiconductor contributes to mitigating the limitations posed by the rapid re-incorporation of electron–hole couples, thereby expanding the potential application of this composite material.

Based on existing research, there is a prominent absence of studies exploring the application of α-Fe_2O_3/MgO nanocomposites for the photocatalytic degradation of organic pollutants, specifically rose Bengal (RB) dye, in a neutral medium. This article is primarily dedicated to the use of a user-friendly hydrothermal method for the synthesis of an α-Fe_2O_3/MgO nanocomposite, with a comprehensive analysis of its structural, morphological, magnetic, and optical properties. The photocatalytic potential of RB dye is also investigated, revealing its effectiveness as a promising photocatalyst, particularly when exposed to ultraviolet light.

Experimental

Materials Used

The materials used for the synthesis of the α-Fe_2O_3/MgO nanocomposite were $Fe(NO_3)_3{\cdot}9H_2O$ (Sigma Aldrich, 99%), $Mg(NO_3)_3{\cdot}9H_2O$ (Alfa Aesar, 99.9%), urea ($CO(NH_2)_2$; Sigma Aldrich, 99%), and distilled water. The initial step entailed synthesizing pure α-Fe_2O_3 and MgO nanoparticles, after which the nanocomposite was created by combining these two components.

Synthesis Method for α-Fe_2O_3 and MgO Nanoparticles

The production of α-Fe_2O_3 nanoparticles employed a straightforward hydrothermal method. Initially, 6 mmol of $Fe(NO_3)_3{\cdot}9H_2O$ and 8 mmol of $CO(NH_2)_2$ were dissolved in 50 mL of double-distilled water with vigorous agitation. Following a 45-min incubation at ambient temperature, the solution was transferred to a 150-mL Teflon-lined stainless steel autoclave for a hydrothermal reaction at 140°C for 4 h. Upon completion of the reaction, the autoclave was gradually cooled to room temperature. The resulting precipitates were then separated from the solution via centrifugation and underwent multiple washes with distilled water and ethanol.

For the synthesis of MgO, a homogeneous solution was created by dissolving $Mg(NO_3)_3{\cdot}9H_2O$ and $CO(NH_2)_2$ in distilled water. After 20 min of stirring, the solution was transferred to a Teflon-lined stainless steel autoclave for an 8-h hydrothermal reaction at 180°C. Subsequently, the autoclave was turned off, and the Teflon beaker was allowed to cool to room temperature. The obtained precipitates were collected, washed with distilled water and ethanol to remove impurities, and then calcined for 3 h at 500°C in a furnace to produce MgO nanoparticles.

Synthesis Method for the α-Fe_2O_3/MgO Nanocomposite

A novel hydrothermal technique was utilized to synthesize the α-Fe_2O_3/MgO nanocomposite as depicted in Fig. 1. In the initial step, a solution was formed by dissolving $Mg(NO_3)_3{\cdot}6H_2O$ and $CO(NH_2)_2$ in double-distilled water under continuous stirring at room temperature. α-Fe_2O_3 nanoparticles were then added to the solution. The resulting mixture underwent hydrothermal treatment in a 150-mL Teflon-lined stainless steel autoclave at 150°C for 8 h. The precipitates obtained were washed multiple times with

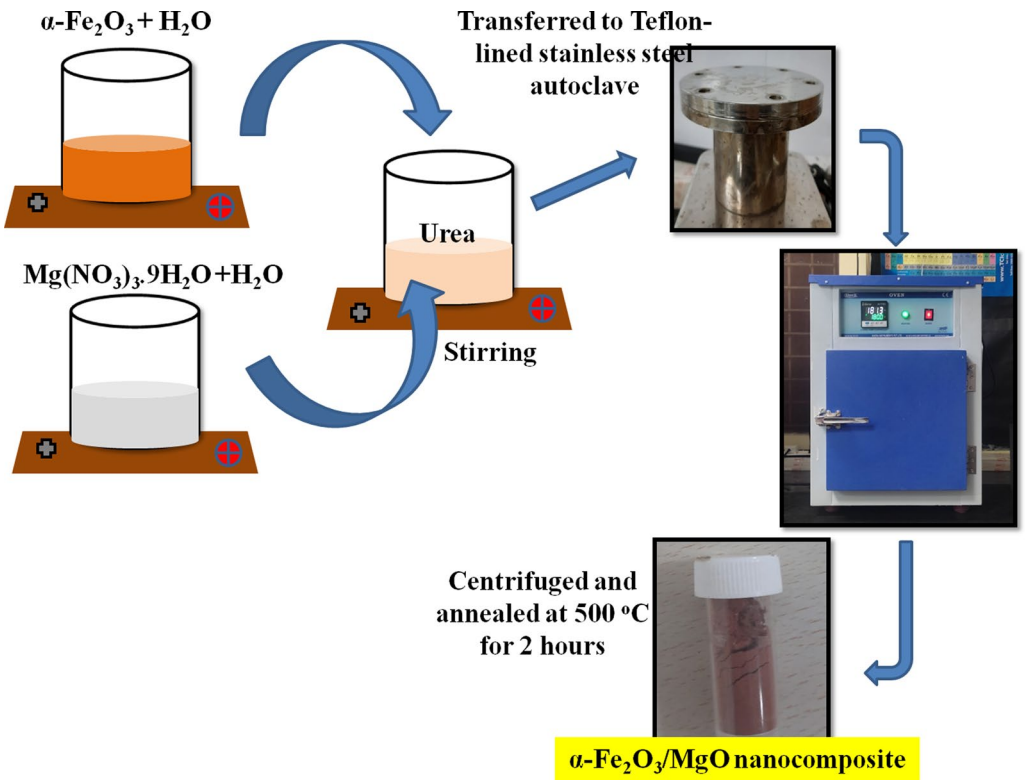

Fig. 1 Schematic representation of hydrothermal synthesis of α-Fe_2O_3/MgO nanocomposite.

double-distilled water and ethanol, followed by drying at 80 °C for 2 h. Finally, the synthesized samples were annealed at 500°C for 2 h to obtain the desired nanocomposite.

Characterization Techniques

A Rigaku Ultima IV diffractometer (DCRUST) equipped with a Cu-K_α source was employed to conduct x-ray diffraction (XRD) analysis on the synthesized samples. Morphological features were examined via high-resolution transmission electron microscopy (HRTEM) using a Tecnai G2 20 instrument located at the All India Institute Of Medical Sciences (AIIMS), New Delhi. The magnetic properties of the synthesized materials were assessed using vibrating sample magnetometry (VSM; MicroSense, ADE-EV9 magnetometer, University of Delhi). Optical specifications, including reflectance and transmittance data, were studied using a Shimadzu UV–visible (UV–Vis) spectrophotometer equipped with a double-beam monochromator (UV-3600 Plus) covering a wavelength range of 200–1100 nm.

Photocatalytic Experiment

The photocatalytic efficiency of the synthesized samples was assessed by degradation of RB dye. To initiate the experiments, a specific quantity of the photocatalyst was dispersed into a 50-mL solution of RB dye with continuous stirring for 30 min, without exposure to irradiation from a UV lamp (300 W). After reaching equilibrium, the light source was activated to commence the photocatalytic reactions. At specific intervals of irradiation, a 2-mL aliquot was extracted, and the UV–Vis spectrophotometer was employed to monitor RB dye concentration.

Results and Discussion

X-ray Diffraction Analysis

The particle crystallinity of α-Fe_2O_3 and MgO was assessed through XRD analysis as shown in Fig. 2. In the XRD spectra of α-Fe_2O_3, prominent peaks were observed at 24.2°, 33.1°, 35.4°, 40.8°, 49.4°, 54.1°, 57.7°, 62.4°, and 64.1°, which corresponded to pure hematite nanoparticles, as identified by JCPDS card no. 33-0664.[16] The presence of narrow, sharp, and intense peaks confirmed the crystallinity of α-Fe_2O_3. In the XRD analysis of the MgO nanoparticles, four peaks were noted at 2θ values of 36.8°, 42.7°, 62.2°, and 74.5°, indicating the characteristic pattern of MgO according to JCPDS card 87-0653.

The presence of certain diffraction peaks in XRD patterns enabled the identification of crystal phases and the evaluation of their composition in the nanocomposite by modifying

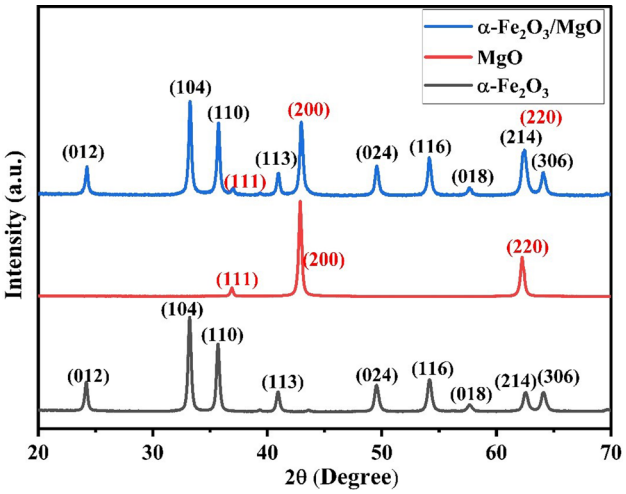

Fig. 2 XRD pattern of synthesized α-Fe_2O_3, MgO, and α-Fe_2O_3/MgO nanocomposite.

Table I Parameters calculated from XRD patterns of synthesized samples

Sample	Crystallite size (nm)	Lattice parameter (Å)		
		MgO	α-Fe_2O_3	
		a = b = c (Å)	a = b (Å)	c (Å)
MgO	23.8	4.21	–	
α-Fe_2O_3	24.8	–	5.15	13.65
α-Fe_2O_3/MgO	26.8	4.19	5.01	13.70

their properties. The effective fabrication of the metal oxide nanocomposite was validated by the co-occurrence of α-Fe_2O_3 and MgO peaks in the nanocomposite. The absence of additional peaks in the XRD spectra of α-Fe_2O_3 and MgO indicated the high phase purity of the synthesized samples. The Debye–Scherrer equation was employed to determine the average crystal size of synthesized α-Fe_2O_3, MgO, and α-Fe_2O_3/MgO. The calculated data revealed an approximate average crystallite size of 24.8 nm for α-Fe_2O_3, 23.8 nm for MgO, and 26.8 nm for the α-Fe_2O_3/MgO nanocomposite, confirming the nanoscale dimensions of the synthesized samples, as given in Table I. The α-Fe_2O_3/MgO nanocomposite contained all the peaks of α-Fe_2O_3 and MgO only, showing the successful formation of the nanocomposite.

For the rhombohedral structure of α-Fe_2O_3, Eq. 1 can be used to obtain the lattice parameters (a = b ≠ c):

$$\frac{1}{d_{hkl}^2} = \frac{h^2 + k^2}{a^2} + \frac{l^2}{c^2}. \quad (1)$$

The peak positions in the XRD pattern are determined by the interplanar spacing of the crystal lattice and can be expressed in terms of Bragg's law:

$$n\lambda = 2d\sin(\theta), \tag{2}$$

where d is the interplanar spacing, (h, k, l) represents Miller indices, and θ denotes diffraction angles.[17]

HRTEM Analysis

This detailed investigation utilizes HRTEM to examine the morphological properties and particle size of the synthesized samples. Specifically, the study concentrates on evaluating pure α-Fe_2O_3, MgO nanoparticles, and the α-Fe_2O_3/MgO nanocomposite. The HRTEM images depicted in Fig. 3 display the morphology of the synthesized nanoparticles, which exhibit a spherical shape for both pure α-Fe_2O_3 and MgO nanoparticles and for the α-Fe_2O_3/MgO nanocomposite. This uniformity in morphology persists across various samples, evident in the images presented in Fig. 3a–c. The particle size histograms situated under the HRTEM images in Fig. 3 reveal average particle size ranging from 19 nm to 30 nm, indicating some variability across the samples.

FTIR Analysis

Figure 4 depicts the Fourier transform infrared (FTIR) spectra of the synthesized samples, covering the wave number range of 400–4000 cm^{-1}, enabling the identification of chemical bonds and functional groups. The significant broadband signals observed at 3416.79 cm^{-1} and 3461.11 cm^{-1} are attributed to the stretching vibration of the hydroxyl (O–H) group in α-Fe_2O_3 and MgO, respectively. In the case of pure α-Fe_2O_3, the absorption peak at 1545.87 cm^{-1} correlates with the bending motion of the O–H) group. Peaks occurring

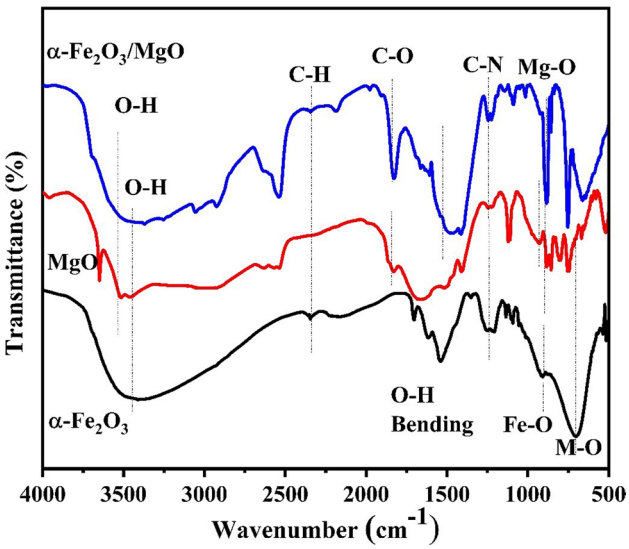

Fig. 4 FTIR patterns of synthesized α-Fe_2O_3, MgO, and α-Fe_2O_3/MgO nanocomposite.

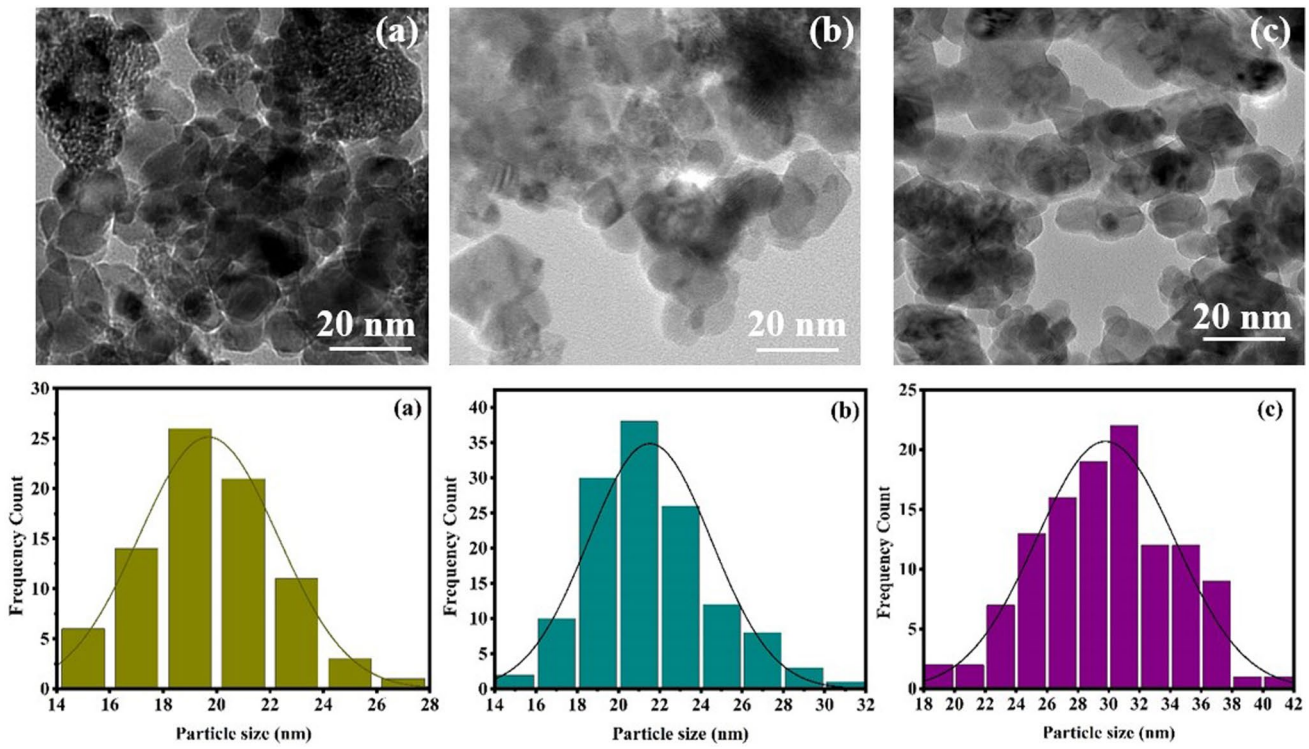

Fig. 3 HRTEM images of (a) α-Fe_2O_3, (b) MgO, and (c) α-Fe_2O_3/MgO nanocomposite with histograms of the particle size distribution in each image.

in the range of 908.24–461.33 cm^{-1} and at 1351.47 cm^{-1} in pure α-Fe_2O_3 correspond to Fe–O stretching and vibration of C–N bonds, respectively.[18] Additionally, the peaks at 2346.81 cm^{-1} and 1704.51 cm^{-1} indicate the stretching of C–H bonds and C–O bonds, respectively. For MgO nanoparticles, the prominent peak detected at 3461.11 cm^{-1} can be attributed to the stretching mode of O–H groups, indicating the presence of hydroxyl groups predominantly on the surface due to moisture. Similarly, the peak detected at 1510.88 cm^{-1} is ascribed to the bending vibration of water molecules. The peak in the region between 932.34 cm and 516 cm^{-1} is assigned to Mg–O stretching vibrations. The FTIR spectrum of the α-Fe_2O_3/MgO nanocomposite depicted in Fig. 3c displays bands between 887.24 cm^{-1} and 639.19 cm^{-1}, indicative of metal oxide (M–O) bonds. In addition, peaks observed at 3374.80 cm^{-1} and 1472 cm^{-1} correspond to the stretching and bending vibrations of H_2O molecules, respectively, likely absorbed from the surroundings.[19] All the peaks corresponding to the individual components of α-Fe_2O_3 and MgO are present in the α-Fe_2O_3/MgO nanocomposite spectrum, indicating the successful synthesis of the nanocomposite.

UV–Vis Spectroscopic Analysis

UV–Vis spectroscopy was utilized to assess the bandgap of α-Fe_2O_3, MgO, and the α-Fe_2O_3/MgO nanocomposite, as shown in Fig. 5. The optical bandgap values of both pure samples and the synthesized nanocomposite can be determined by Tauc plots, where the absorption edge is extrapolated to the energy axis using the following equation:

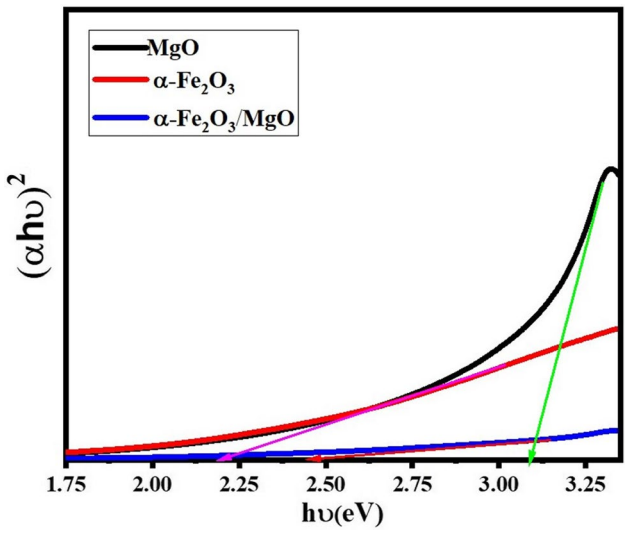

Fig. 5 Tauc plots for α-Fe_2O_3, MgO, and α-Fe_2O_3/MgO nanocomposite.

$$(\alpha h\upsilon)^n = A\left(h\upsilon - E_g\right). \tag{3}$$

The Tauc plot is analyzed to determine the optical bandgap (E_g), wherein A, α, and hυ represent the constant, absorption coefficient, and photon energy, respectively.[20]

Plotting the quantity $(\alpha h\upsilon)^n$ against the photon energy (hυ) yields the bandgap energy. Bandgap energy values of 2.2 eV and 3.08 eV are found for pure α-Fe_2O_3 and MgO nanoparticles, respectively, as shown in Fig. 5. Upon decorating α-Fe_2O_3 onto MgO, the bandgap value shifts to 2.45 eV for the α-Fe_2O_3/MgO nanocomposite. This change in bandgap value is ascribed to the effective surface modification of pure samples with the nanocomposite, indicating an electrical transition between the two components and suggesting that the synthesized nanocomposite facilitates effective absorption of UV light.

Additionally, the valence band (VB) position was computed utilizing the following equation:

$$E_{VB} = \chi - E_e + 0.5E_g \tag{4}$$

Subsequently, the conduction band (CB) energy was determined using the formula $E_{CB} = E_{VB} - E_g$. Here, χ is the absolute electronegativity of the photocatalyst, and E_e is the free electron energy in the hydrogen scale (4.5 eV).[21,22] For α-Fe_2O_3 and MgO, χ values of 5.87 eV and 5.68 eV were found, respectively.[23,24] The values determined for the valence band and conduction band sites are presented in Table II. This configuration has the potential to enhance photocatalytic efficacy by prolonging the recombination time of excitons.

VSM Analysis

Figure 6 displays the magnetic hysteresis loops for pure α-Fe_2O_3 and MgO nanoparticles and their nanocomposite. Magnetic parameters including saturation magnetization (M_s), coercivity (H_c), remanence (M_r), and squareness factor (S) were quantified.[25] The saturation magnetization (M_s) values for α-Fe_2O_3, MgO, and the α-Fe_2O_3/MgO nanocomposite at a magnetic field strength of 10,000 Oe are 1.5, 5.0×10^{-3}, and 0.3 Oe, respectively. The remanence magnetization (M_r) and coercivity (H_c) values for α-Fe_2O_3, MgO, and the α-Fe_2O_3/MgO nanocomposite are presented in Table III. According to Stoner and Wohlfarth, a squareness

Table II Results calculated from UV–Vis spectroscopy

Sample	Bandgap (eV)	E_e (eV)	χ (eV)	E_{VB} (eV)	E_{CB} (eV)
α-Fe_2O_3	2.20	4.5	5.87	2.47	0.27
MgO	3.08	4.5	5.68	2.72	−0.36

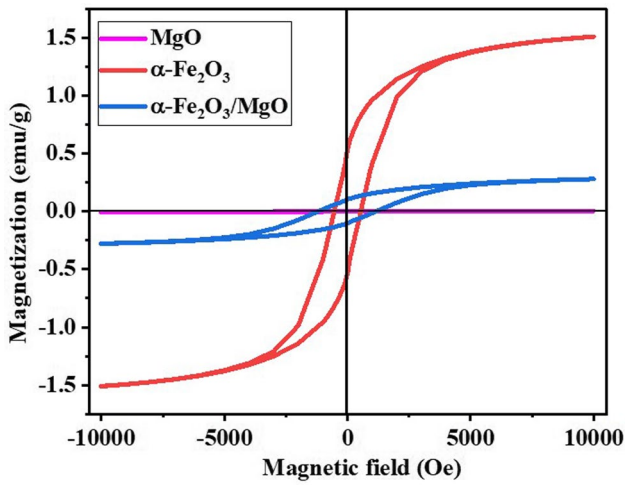

Fig. 6 Magnetization curves of synthesized α-Fe_2O_3, MgO, and α-Fe_2O_3/MgO nanocomposite.

Table III Saturation magnetization, coercivity values, retentivity, and squareness ratio values of magnetic hysteresis loop for synthesized samples

Sample	Magnetization (M_s), emu/g	Coercivity value (H_c), Oe	Retentivity (M_r), emu/g	Squareness ratio (M_r/M_s)
α-Fe_2O_3	1.5	588.2	0.5	0.33
MgO	5.0×10^{-3}	889.2	2.5×10^{-3}	0.50
α-Fe_2O_3/MgO	0.3	1064.7	0.1	0.33

factor (S) of 0.5 indicates that the particles are oriented randomly and do not interact, whereas $S<0.5$ indicates that the particles are engaged in magnetostatic interactions. The observation that the squareness value is less than 0.5 in synthesized samples shows the presence of magnetostatic interaction among the particles.[26]

A comparison of the VSM curves reveals that the saturation magnetization for the synthesized nanocomposite decreases due to surface modification, indicating the growth of MgO on the α-Fe_2O_3 surfaces related to strain and lattice distortion. This effect can be attributed to the presence of weakly magnetic MgO in the total sample volume. The magnetism observed in MgO nanoparticles arises primarily from defect-induced effects in the sample. Li et al. investigated MgO nanoparticles and noted ferromagnetism, which they attributed to the presence of Mg vacancies.[27] Similarly, several other studies have reported that while bulk MgO exhibits nonmagnetic properties, MgO nanocrystals exhibit ferromagnetism at room temperature, likely due to the creation of Mg vacancies or the donation of charges by oxygen atoms, leading to the formation of 2*p* holes at the surface of the nanograins. Bishno et al.[28] investigated defect-induced magnetism in MgO using first-principles calculations and proposed that the induced magnetic moment results from the spin polarization of 2*p* electrons of oxygen atoms near Mg vacancies. These calculations indicated that pure MgO in bulk form lacks magnetic properties.

Photocatalytic Activity

Assessment of Photodegradation Efficiency

The prepared samples were examined for their ability to catalyze the degradation of rose Bengal (RB) dye under UV light. To achieve equilibrium between adsorption and desorption, a precise quantity of photocatalyst was dispersed in 50 mL of RB dye solution and stirred continuously for 30 min. Once equilibrium was reached, the light source was activated to initiate the photocatalytic experiments. A 2-mL sample was extracted at specific intervals of radiation exposure, followed by centrifugation for 5 min to eliminate the photocatalyst particles for evaluation.

Certain factors, such as surface area, generation of OH• radicals, and efficiency of electron–hole pair separation, play a crucial role in the performance of photocatalysts. Beer's law establishes a direct correlation between the concentration of a substance and its absorption, and is utilized to ascertain the efficiency of degradation:

$$\%\text{degradation} = \left(C_0 - C\right)/C_0 * 100 \quad (5)$$

herein, C_0 represents the initial concentration of dye at time zero, while C denotes the concentration of dye at any given time t.[29]

The effectiveness of the synthesized materials' photocatalytic capabilities was assessed by monitoring the variation in RB dye concentration over time under exposure to UV light. Figure 7 displays the absorbance spectra, illustrating the degradation of RB dye within the range of 400–700 nm for all synthesized samples. The percentage degradation efficiency of the RB dye was computed and is depicted for all samples in Fig. 8. The percentage degradation achieved after UV light exposure for 75 min was as follows: α-Fe_2O_3 (74%), MgO (81%), and α-Fe_2O_3/MgO (84%), as illustrated in Fig. 8c. The α-Fe_2O_3/MgO nanocomposite exhibited the most significant degradation efficiency when compared to the pure nanoparticles.

The α-Fe_2O_3 material possesses bandgap energy of 2.2 eV, resulting in rapid recombination of electrons and holes, thus leading to decreased photocatalytic degradation activity towards RB dye. Conversely, the limited efficiency of MgO nanoparticles stems from their high bandgap energy, which restricts the production of electron–hole pairs and

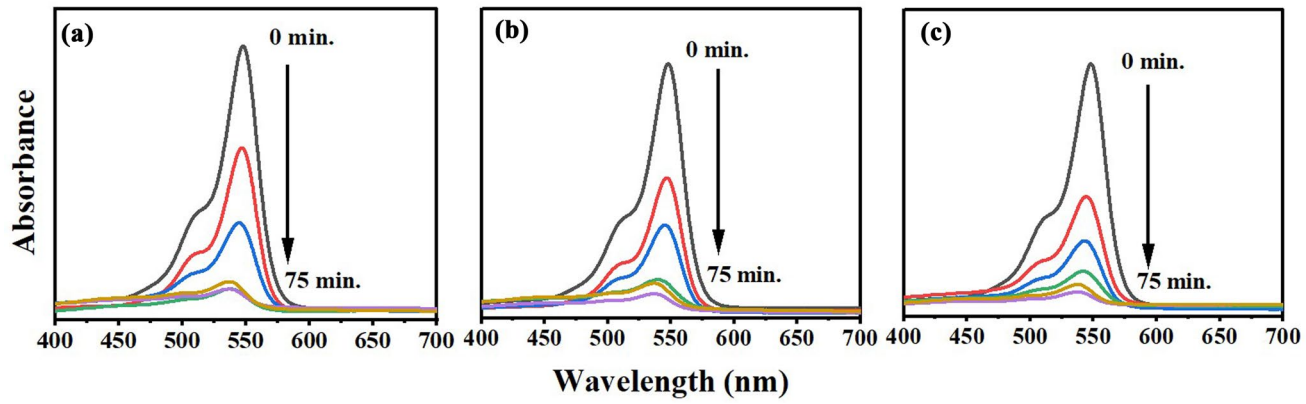

Fig. 7 Absorption spectra of RB dye at various durations under exposure to UV light using (a) α-Fe_2O_3, (b) MgO, (c) α-Fe_2O_3/MgO nanocomposite.

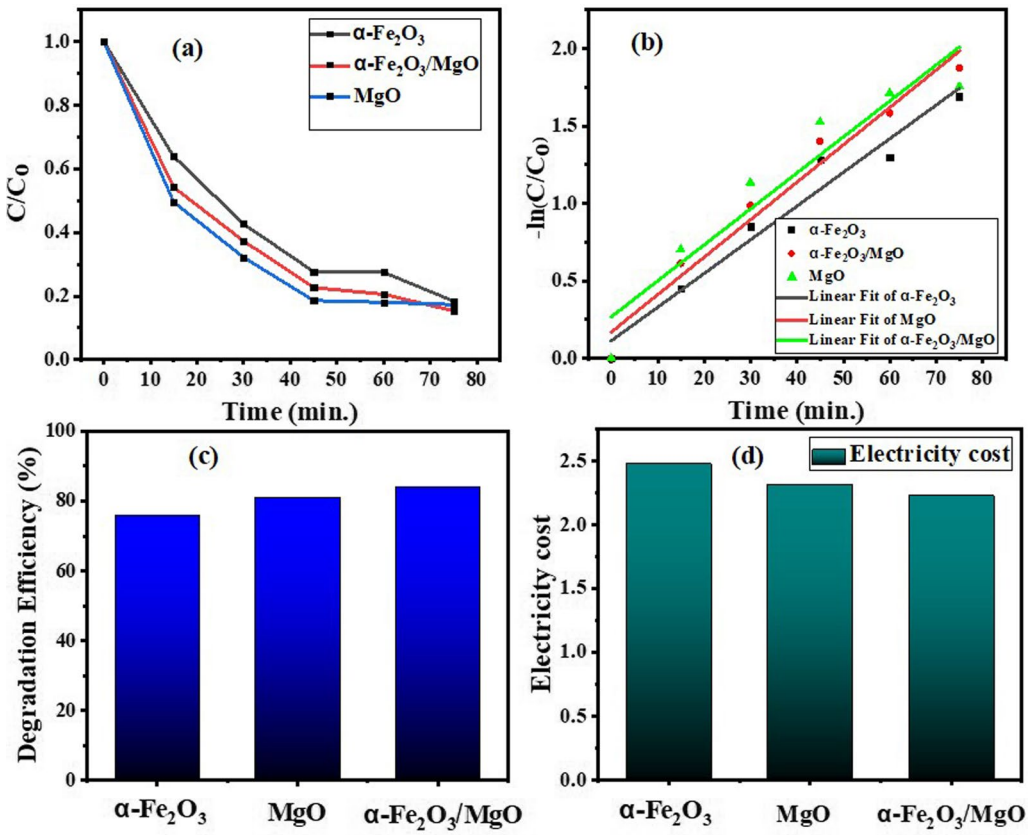

Fig. 8 (a) Relative dye concentration versus exposure time, (b) linear fitting of exposure time and ln(C/C_0), (c) percentage degradation of synthesized samples, and (d) electricity cost (in INR) of α-Fe_2O_3, MgO, and α-Fe_2O_3/MgO nanocomposite.

reactive species due to the minimal excitation by irradiated photons. However, this drawback can be addressed by incorporating α-Fe_2O_3 with MgO to form a nanocomposite. The formation of heterojunctions in these nanocomposites facilitates better separation of electron–hole pairs, enhancing the mobility of charge carriers.

Furthermore, the linear plot of ln(C/C_0) against time indicates first-order kinetics, a conclusion later supported by the values of R^2, where R^2 represents the linear correlation coefficient.[30] The high R^2 values in the dye degradation process, nearing 1, strongly suggest pseudo-first-order kinetics, as indicated in Table IV. Thus, a first-order

model was employed to analyze the entire photocatalytic mechanism:

$$\ln\left(C/C_0\right) = -kt \tag{6}$$

The rate constant values derived from the kinetics plots for each sample are depicted in Fig. 8b. For the synthesized catalysts (α-Fe_2O_3, MgO, α-Fe_2O_3/MgO nanocomposite), k was calculated from the slope of the linear fit, yielding rate constants of 0.0217, 0.0232, and 0.0241 min^{-1}, respectively. Significantly, the rate constant values increase in the nanocomposite, reaching their highest value.

Cost of Electricity

The electricity cost provides an estimate of the amount of electrical energy needed for the degradation of a dye. The estimated amount of time needed for the degradation of RB dye to 90% of its initial concentration was evaluated (listed in Table IV) using the following relation[31]:

Table IV Parameters determined from photocatalytic degradation of RB dye using α-Fe_2O_3, MgO, and α-Fe_2O_3/MgO nanocomposite

Sample	Percentage degradation in 75 min	K (min^{-1})	R^2	t_{90}	E_C (INR)
α-Fe_2O_3	76	0.0217	0.999	105	2.97
MgO	81	0.0232	0.995	99	2.31
α-Fe_2O_3/MgO	84	0.0241	0.989	95	2.22

$$t_{90} = \frac{\ln(10)}{K} \tag{7}$$

In addition, using synthesized samples, the cost of electricity (E_C) to degrade RB dye was estimated using the following relations[32]:

$$E_C = \frac{P \times t_{90} \times 4.68}{1000 \times 60} \tag{8}$$

where P denotes the power of the UV light source, V denotes the volume, and t_{90} is the length of time it takes for the dye to degrade to 90% of its original concentration. With maximum consumption of 500 units, the cost of electricity in our locality is 4.68 Indian rupees (INR) per unit.[33] The electricity cost decreases from α-Fe_2O_3 to α-Fe_2O_3/MgO, as shown by Fig. 8d and Table IV.

Based on the findings of the above photocatalytic studies, two primary factors are obtained that positively influenced the photocatalytic activity: firstly, the inhibition of recombination of photogenerated charge carriers achieved through the formation of heterojunctions, and secondly, the particle morphology of the photocatalysts.

Mechanism

Figure 9 illustrates the photodegradation process of RB dye utilizing α-Fe_2O_3, MgO, and the α-Fe_2O_3/ MgO nanocomposite. Table II presents the bandgaps, conduction bands, and valence bands of α-Fe_2O_3 and MgO. The bandgap of MgO (3.08 eV) surpasses that of α-Fe_2O_3 and the α-Fe_2O_3

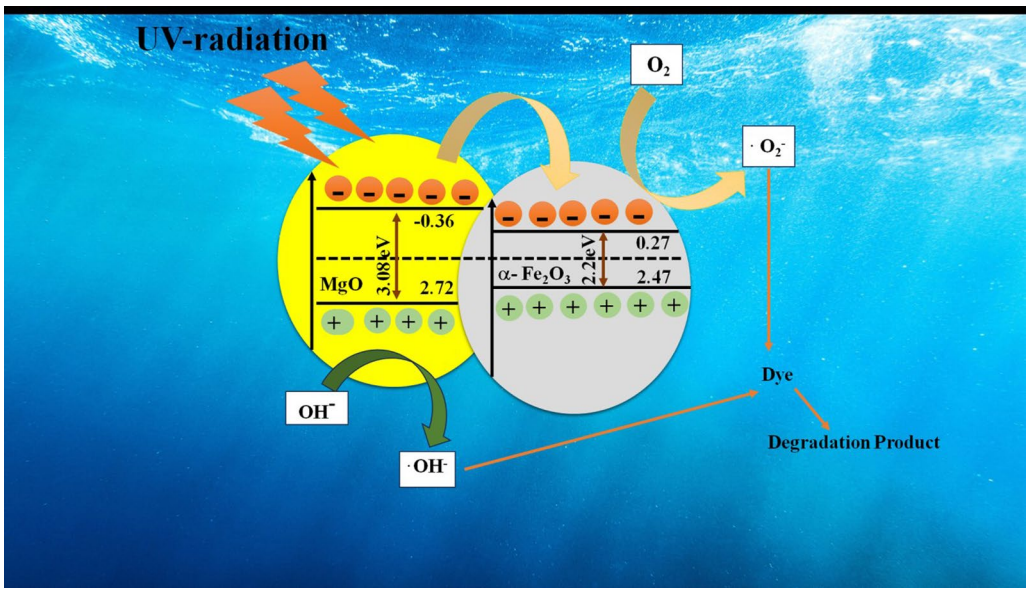

Fig. 9 Photocatalytic dye degradation mechanism of α-Fe_2O_3/MgO nanocomposite.

/MgO nanocomposite, implying that MgO is able to absorb a wide spectrum of light, and this energy can be used for degrading dye molecules in water. The proposed mechanism for the photodegradation of RB by the nanocomposite under UV light irradiation is depicted in Fig. 9, illustrating the concurrent excitation of the synthesized nanocomposite, resulting in the generation of electrons in the conduction band and holes in the valence band.

The introduction of α-Fe_2O_3 nanoparticles onto the MgO nanostructures results in the formation of a heterojunction barrier at the interface between the metal oxide and the semiconductor. This barrier arises from the difference between the work functions of MgO and α-Fe_2O_3. Under UV radiation exposure, MgO absorbs light, leading to the movement of electrons (e^-) from the valence band to the conduction band and the generation of an equivalent number of holes (h^+) in the valence band. The electrons resulting from this photolytic process in the conduction band of MgO then migrate to the conduction band of α-Fe_2O_3. The limited diffusion length hinders the transfer of photogenerated holes from MgO to α-Fe_2O_3, and they remain confined to the surface of MgO. The segregation of holes and photogenerated electrons results in a decrease in their recombination rate. Hydroxyl radicals (OH•) are generated through the oxidation of water molecules by the persistent positive hole. Additionally, highly reactive superoxide radicals (O^{2-}) are formed as electrons and are captured by dissolved oxygen in water. These hydroxyl (OH•) radicals facilitate the breakdown of RB dye into CO_2 and other by-products.

Assessing the Reusability of the α-Fe_2O_3/MgO Nanocomposite as a Photocatalyst for Dye Degradation

A crucial aspect of adopting eco-friendly practices hinges on the ability of catalysts to be reused. Photocatalysts play a vital role in dye degradation, exhibiting peak performance when they exhibit both stability and recoverability. According to the study, the α-Fe_2O_3-MgO nanocomposite emerged as the most promising photocatalyst among all synthesized samples. To evaluate its reusability, the nanocomposite underwent testing over four cycles. The results, depicted in Fig. 10, indicate stability, with a decrease of approximately 4% in dye degradation efficiency during the third cycle and around 7% during the fourth cycle. These declines are due to the decreased magnetic characteristics of the nanocomposite and also suggest that the material maintains its reduced potential for further reuse.

Previous work done so far:

Here's a tabular form comparing previous work done on α-Fe_2O_3/MgO nanocomposites in photocatalytic activity (Table V).

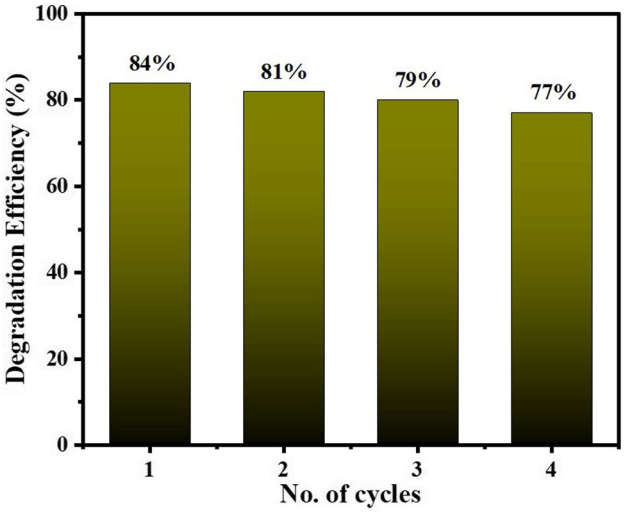

Fig. 10 Reusability performance of α-Fe_2O_3/MgO nanocomposite for the degradation of RB dye.

Conclusion

This study employed a cost-efficient hydrothermal route to synthesize an α-Fe_2O_3/MgO nanocomposite tailored for wastewater treatment applications. The utilization of hydrothermal synthesis ensures economical production while maintaining precise control over nanoparticle morphology and composition. Comprehensive characterization techniques, including XRD and HRTEM, confirmed the successful formation of the nanocomposite. HRTEM analysis revealed nanocrystalline particles within the size range of 19 nm to 30 nm, indicative of the desired nanostructure. UV–Vis spectroscopy further elucidated the optical properties of the nanocomposite, revealing a tunable bandgap ranging from 2.20 eV to 3.08 eV. This modifiable bandgap signifies the incorporation of wide-bandgap semiconductor materials, essential for efficient photocatalytic activity. Assessment of the magnetic properties via VSM reveals a discernible reduction in magnetization in the nanocomposite, attributed to the incorporation of nonmagnetic MgO into the magnetic α-Fe_2O_3 matrix.

Notably, the α-Fe_2O_3/MgO nanocomposite demonstrates remarkable photocatalytic activity, achieving an impressive 84% degradation of rose Bengal (RB) dye under UV irradiation within a mere 75-min timeframe. This observation underscores the nanocomposite's potential as a highly effective agent for wastewater treatment, showcasing its applicability in addressing environmental contaminants of concern.

Table V Tabular form comparing previous work on α-Fe_2O_3/MgO nanocomposite in photocatalytic activity application

Study	Method	Nanocomposite	Target pollutant and time	Photocatalytic efficiency	Reference
1.	Sol-gel method	Zn doped α-Fe_2O_3	Rose bengal, 90 min	87% degradation	[33]
2.	Spray pyrolysis	Mg doped α-Fe_2O_3	Methylene blue, 180 min	98% degradation	[34]
3.	Hydrothermal synthesis	α-Fe_2O_3 doped MgO	Crystal violet, 30 min	98% degradation	[35]
4.	Co-precipitation method	Ni doped α-Fe_2O_3	Methylene blue, 140 min	86% degradation	[36]
5.	Co-precipitation method	SiO_2 doped α-Fe_2O_3	Rhodamine blue, 150 min	91% degradation	[37]
6.	Wet chemical reflux method	Ag doped α-Fe_2O_3	Malachite green, 90 min	98% degradation	[38]
7.	Sol-gel method	Activated carbon Zr doped α-Fe_2O_3	Rhodamine 6G, 90 min	77.98% degradation	[39]
8.	Hydrothermal method	α-Fe_2O_3 doped MgO	Rose bengal, 75 min	84% degradation	This work

Author Contributions Data collection and analysis: S., M., V.A. Visualization and supervision: Dr. S.C., M.K.S. Formal analysis, Editing: R.K., H.K., S.S.

Data Availability Data will be made available on request.

Conflict of interest The authors declare that they are not aware of any personal or financial conflicts that might have appeared to affect the research reported in this study.

References

1. S.G. Menon, A.K. Bedyal, T. Pathak, V. Kumar, and H.C. Swart, $Sr_4Al_{14}O_{25}$: Eu^{2+}, Dy^{3+}@ZnO nanocomposites as highly efficient visible light photocatalysts for the degradation of aqueous methyl orange. *J. Alloys Compd.* 860, 158370 (2021).
2. R.P. Schwarzenbach, T. Egli, T.B. Hofstetter, U. Von Gunten, and B. Wehrli, Global water pollution and human health. *Annu. Rev. Environ. Resour.* 35, 109 (2010).
3. H. Kumari, Sonia, S. Sharma, S. Chahal, M. Gupta, A. Kumar, R. Parmar, Enhanced catalytic degradation of organic dye by $Sn_{1-x}La_xO_2$ nanoparticles under UV light for wastewater treatment, J Photochem Photobiol A Chem 453, 115673 (2024)
4. H. Kumari, Sonia, S. Chahal, Suman, P. Kumar, A. Kumar, R. Parmar, Photocatalytic Degradation of RB dye via Cerium substituted SnO_2 Photocatalysts. Mater. Sci. Eng. B. 296, 116654 (2023).
5. G.D. Sharma, P. Balraju, M. Kumar, and M.S. Roy, Quasi solid state dye sensitized solar cells employing a polymer electrolyte and xanthene dyes. *Mater. Sci. Eng. B* 162, 32 (2009).
6. G. Rammohan and M. Nadagouda, Green photocatalysis for degradation of organic contaminants: a review. *Curr. Org. Chem.* 17, 2338 (2013).
7. R. Kant, Textile dyeing industry an environmental hazard. *Nat. Sci.* 4, 22 (2012).
8. S.T. Fardood, F. Moradnia, F.Y. Zare, S. Heidarzadeh, M.A. Majedi, A. Ramazani, M. Sillanpää, and K. Nguyen, Green synthesis and characterization of α-Mn_2O_3 nanoparticles for antibacterial activity and efficient visible-light photocatalysis. *Sci. Rep.* 14, 6755 (2024).
9. P. Bhayana, T. Dandekar, R. Bala, R. Madaan, and P. Mahajan, Role of carbon nanotubes in remediation of pharmaceutical wastewater. *Remediation* 34, 21776 (2024).
10. P. Dhiman, G. Rana, A. Kumar, G. Sharma, D.V.N. Vo, and M. Naushad, ZnO-based heterostructures as photocatalysts for hydrogen generation and depollution: a review. *Environ. Chem. Lett.* 20, 1047 (2022).
11. R. Thiruvenkatachari, S. Vigneswaran, and I.S. Moon, A review on UV/TiO_2 photocatalytic oxidation process (Journal Review). *Korean J. Chem. Eng.* 25, 64 (2008).
12. A. Belghit, S. Merouani, O. Hamdaoui, M. Bouhelassa, and S. Al-Zahrani, The multiple role of inorganic and organic additives in the degradation of reactive green 12 by UV/chlorine advanced oxidation process. *Environ. Tech.* 43, 835 (2022).
13. M.Y. Guo, A.M.C. Ng, F. Liu, A.B. Djurišić, and W.K. Chan, Photocatalytic activity of metal oxides-The role of holes and OH• radicals. *Appl. Catal. B* 107, 150 (2011).
14. M. Parashar, V.K. Shukla, and R. Singh, Metal oxides nanoparticles via sol–gel method: a review on synthesis, characterization and applications. *J. Mater. Sci. Mater. Electron.* 31, 3729 (2020).
15. K. Kannan, D. Radhika, K.K. Sadasivuni, R. Reddy, and A.V. Raghu, Historical Perspective Nanostructured metal oxides and its hybrids for photocatalytic and biomedical applications. *Adv. Colloid Interface Sci.* 281, 103178 (2020).
16. Structural and optical properties of α-Fe2O3/ZnO nanocomposite in wastewater treatment. Indian *J. Pure Appl. Phys.* 61, 723 (2023).
17. A. Sonia and P. Kumar, Kumar, Efficient $CoFe_2O_4$/CeO_2 nanocomposites for photocatalytic dye degradation. *J. Mater. Sci. Mater. Electron.* 34, 1870 (2023).
18. S.T. Navale, G.D. Khuspe, M.A. Chougule, and V.B. Patil, Polypyrrole, α-Fe_2O_3 and their hybrid nanocomposite sensor: an impedance spectroscopy study. *Org. Electron.* 15, 2159 (2014).
19. F. Allawi, A.M. Juda, and S.W. Radhi, Photocatalytic degradation of methylene blue over MgO/α-Fe_2O_3 nano composite prepared by a hydrothermal method. *AIP Conf. Proc.* 2290, 030020 (2020).
20. C.J. Li, J.N. Wang, B. Wang, J.R. Gong, and Z. Lin, A novel magnetically separable TiO_2/$CoFe_2O_4$ nanofiber with high photocatalytic activity under UV-vis light. *Mater. Res. Bull.* 47, 333 (2012).
21. A. Sonia and P. Kumar, Kumar, Z-scheme $ZnFe_2O_4$/CeO_2 nanocomposites with enhanced photocatalytic performance under UV light. *Appl. Phys. A Mater. Sci. Process.* 129, 724 (2023).
22. S. Vishwanathan and S. Das, Glucose-mediated one-pot hydrothermal synthesis of hollow magnesium oxide-zinc oxide (MgO-ZnO) microspheres with enhanced natural sunlight photocatalytic activity. *Environ. Sci. Pollut. Res.* 30, 8512 (2023).
23. M.A. Ben Aissa, A. Modwi, K. Taha, N. Elamin, R.A. AbuMousa, M. Bououdina, Environmental remediation applications of MxOy-gC_3N_4 nanocomposites (M = Mg, Ti, and Zn): Photocatalytic activity for Indigo carmine dye degradation. *Diam. Relat. Mater.*, 136, 109988 (2023).

24. S. Zhang, L. Zhou, Y. Hu, X. Liu, and J. Zhang, Metal-organic gel derived ZnO/α-Fe_2O_3 heterostructures for sensitive NO_2 detection. *Sens. Actuators B Chem.* 396, 134324 (2023).
25. P. Sonia and A. Kumar, Kumar, Multifunctional $CoFe_2O_4$/ZnO nanocomposites: probing magnetic and photocatalytic properties. *Nanotechnology* 35, 14 (2024).
26. H. Kumari, Sonia, S. Chahal, Suman, P. Kumar, A. Kumar, R. Parmar, Sol–gel synthesis and characterization of Gd-doped SnO_2 nanoparticles for water treatment and spintronic applications. *J. Mater. Sci. Mater. Electron.* 35, 212 (2024).
27. Q. Li, H. Yuan, Y. Zhang, W. Yan, S. Zhang, B. Liao, and M. Ying, Enhanced room-temperature ferromagnetism in Co and Er co-implanted MgO film. *Mater. Lett.* 333, 133646 (2023).
28. P. Bishnoi, A. Kumar, R. Brajpuriya, K.P.S. Parmar, A. Sharma, K.H. Chae, and A. Vij, Electronic structure and luminescence studies of Bi doped MgO nanophosphors. *Ceram. Int.* 50, 15657 (2024).
29. X. Xu, A. Dutta, J. Khurgin, V. M. Shalaev, A. Wei, A. Boltasseva, TiN@TiO_2 Core-Shell Nanoparticles as Plasmon-Enhanced Photosensitizers for Photocatalysis, 2020 Conference on Lasers and Electro-Optics (CLEO), 1 (2020).
30. Sonia, H. Kumari, Suman, S. Chahal, S. Devi, S. Kumar, S. Kumar, P. Kumar, A. Kumar, Spinel ferrites/metal oxide nanocomposites for waste water treatment, *Appl. Phys. A Mater. Sci. Process.* 129 (2023).
31. N.N. Mahamuni and Y.G. Adewuyi, Advanced oxidation processes (AOPs) involving ultrasound for waste water treatment: a review with emphasis on cost estimation. *Ultrason. Sonochem.* 17, 990 (2010).
32. S. Chahal, S. Singh, A. Kumar, and P. Kumar, Oxygen-deficient lanthanum doped cerium oxide nanoparticles for potential applications in spintronics and photocatalysis. *Vacuum* 177, 109395 (2020).
33. S. Suman, A. Chahal, and P. Kumar, Kumar, Zn doped α-Fe_2O_3: An efficient material for UV driven photocatalysis and electrical conductivity. *Crystals* 10, 273 (2020).
34. R.B. Ayed, M. Ajili, Y. Piñeiro, B. Alhalaili, J. Rivas, R. Vidu, S. Kouass, and N.K. Turki, Effect of Mg doping on the physical properties of Fe_2O_3 thin films for photocatalytic devices. *Nanomaterials* 12, 1179 (2022).
35. M. Thabet, E. M. Abd El-Monaem, W. R. Alharbi, M. Mohamoud, A. H, Abdel-Aty, I. Ibrahim, M. A. Abdel-Lateef, A. E. Goda, T. A. S. Elnasr, R. Wang, H. Gomaa, Adsorption and photocatalytic degradation activities of a hybrid magnetic mesoporous composite of α-Fe2O3 nanoparticles embedded with sheets-like MgO. *J. Water Process. Eng.* 60, 105192 (2024).
36. A. Lassoued, M. S. Lassoued, S. García-Granda, B., Dkhil, S., Ammar, A., Gadri, Synthesis and characterization of Ni-doped α-Fe_2O_3 nanoparticles through co-precipitation method with enhanced photocatalytic activities. *J. Mater. Sci. Mater. Electron.* 29, 5726 (2018).
37. M. Arshad, M., Abbas, S., Ehtisham-ul-Haque, M. A., Farrukh, A., Ali, H., Rizvi, G. A., Soomro, A., Ghaffar, M., Yameen, M. Iqbal, Synthesis and characterization of SiO_2 doped Fe_2O_3 nanoparticles: Photocatalytic and antimicrobial activity evaluation. *J. Mol. Struct*. 1180, 244 (2019).
38. B.R. Das, S. Jena, and J.P. Dhal, Ag doped α-Fe_2O_3 nanoparticles: synthesis, characterization and application as heterogeneous photocatalyst for removal of organic dye from aqueous media without any oxidizing agents. *J. Indian Chem. Soc.* 98, 100214 (2021).
39. G.M. Sivakumari, R. Rajarajan, and S. Senthilvelan. Naveenkumar, Ultraviolet light driven photocatalytic and antimicrobial activity of activated carbon-zirconium doped α-Fe_2O_3 nanocomposites. *Emergent Mater.* 6, 1243 (2023).